Balancing Current and Efficiency Modelling of Single Switch Active Balancing Systems for Energy Storage Systems

I. Aizpuru, U. Iraola, J.M. Canales, A. Goikoetxea, E. Garayalde

University of Mondragón, 20500 Mondragón, Spain

Abstract- High Power battery packs are a series/parallel connection of single energy storage cells.The series connection of cells affects in the whole battery pack energy and power due to the unbalancing behavior of each different cell. To improve the whole battery pack energy a balancing system is connected. Passive balancing systems are wasteful and do not increase the Battery pack energy during discharge. Active balancing systems are efficient but most topologies add big complexity to the *BMS* work. Single switch active balancing systems are simple and reliable. During this work the main balancing current modelling and efficiency equations are presented for the most important single switch active balancing systems. These expressions permit to evaluate the balancing power of the system, and to know how much energy is balanced during the balancing system process between the *Weak* cell and the *Strong* cells. Experimental validation of each balancing system is implemented to compare balancing power, efficiency and behavior.

Index Terms- Active balancing systems, Battery management systems, Energy conversion, Energy efficiency, Energy storage.

Nomenclature

n	Number of series connected cells []
V_{PACK}	Battery Pack voltage [V]
$V_{B,i}$	*i*thcell voltage [V]
$V_{B,W}$	*Weak*cell voltage [V]
$V_{B,S}$	*Strong*cell voltage(s) [V]
D_{cri}	Critical duty cycle ratio[]
D	Working duty cycle ratio[]
T_s	Switching period [s]
$I_{B,i}$	*i*th cell ideal balancing current [A]
$I_{B,S}$	*Strong*cell ideal balancing current [A]
$I_{B,W}$	*Weak* cell ideal balancing current [A]
$P_{B,i}$	*i*th balancing system ideal power [W]
$P_{B,T}$	Total ideal balancing system power [W]
$I^*_{B,i}$	*i*th cell real balancing current [A]
$I^*_{B,S}$	*Strong*cell real balancing current [A]
$I^*_{B,W}$	*Weak* cell real balancing current [A]
$P^*_{,B,i}$	*i*th balancing system real power [W]
$P^*_{B,T}$	Total balancing system real power [W]
$P_{Loss,T}$	Total balancing system power loss [W]
η	Balancing system efficiency [%]
$V_{PS,i}$	*i*th power supply voltage [V]
$I_{PS,i}$	*i*th power supply current [A]

I. Introduction

Driven by nowadays increase of power and energy demand several continental, national and regional energy strategy plans have been developed with the main issue of decreasing primary energy sources and increase insertion of renewable energies, decrease CO_2 emissions and increase energy efficiency [1], [2].

Energy storage systems *ESS* are the main technology to help increasing the impact of renewable energy, as wind energy and photovoltaic generation[3]–[15], or the insertion of the hybrid and electric car[16]–[21].

Inside *ESS* systems battery based energy systems are one of the most promising technologies. High power battery packs are a series/parallel connection of single battery cells or small battery modules[22]–[27].

Series connection of battery cells have an unbalancing effect in the battery pack, due to differences between cells [28]–[31], inducing a total battery energy and performance reduction[32], [33].

Passive balancing is the most used balancing technique, but it is wasteful and the balancing procedure is only useful during charge process[34]–[36].

Active balancing systems are more efficient but are complex, with high number of switching devices, which increase the price and decreases the competitiveness of these devices[37]–[44].To decrease the complexity of active balancing systems single switch balancing topologies are a great option[45], [46]. A single switch is used to balance all the cells, with the possibility of controlling the active switch with an open loop strategy.

In the present work, a generalized description of main single switch topologies for active balancing systems will be given. The main goal of the present work is to model the current of the active balancing systems shunted from each single cell. It is the main parameter in the design and sizing of the balancing system. The efficiency of the balancing system is also modelled, to know the power loss respected to the ideal current model.

As the first step in section II, main single switch balancing topologies and modelling equations will be presented. These equations are the main part for the balancing system sizing.

In section III, power losses of the single switch balancing circuits are modelled. The power losses of balancing circuits are of great impact and interest in balancing systems because they

manage low balancing power and the losses have big influence on the balancing currents. With the power losses the balancing currents are recalculated.

During section IV, experimental results of real prototypes will be presented and compared to modelling results. Special interest will be presented regarding power losses and efficiency of the prototypes.

Ideal modelling of single switch balancing topologies

Opel loop switching control (no feedback control) is possible in single switch balancing systems guaranteeing the Discontinuous Conduction Mode DCM during the full working range. During the first step the most important issues to guarantee the DCM will be presented. After the main issues of current balancing will be presented to finish with the ideal balancing current models.

Open loop Discontinuous Conduction Mode DCM

Single switch active balancing topologies must guarantee the *DCM* to work in an open loop control mode.

$$\left.\begin{array}{l} T_{ON}+T_{OFF1}+T_{OFF2}=T_S \\ D+D_1+D_2=1 \\ D_2\geq 0 \end{array}\right\}\ \text{DCM} \qquad (1)$$

The critical duty cycle ratio D_{cri} is the maximum working duty cycle $D$to guarantee the DCM. D_{cri} is defined when the value of the zero current period D_2 is zero.

$$D_{cri}=1-D_1,\quad \text{for } D_2=0 \qquad (2)$$

The only requirement to guarantee the DCM mode is to keep$D$ behind or equal to D_{cri}.

$$D\leq D_{cri},\quad \text{for DCM} \qquad (3)$$

I

deal current modelling of single switch balancing topologies

Single switch balancing system topologies perform voltage based balancing. The balancing system equals all the voltages of the series connected cells by the natural topology behavior.

When the voltage is equal in all *n*series connected $V_{B,i}$cells, no balancing current $I_{B,i}$is injected nor extracted from the cells.

$$V_{B,1}=V_{B,2}=...=V_{B,n-1}=V_{B,n},\qquad I_{B,i}=0 \qquad (4)$$

When a voltage unbalance occurs, the cell with the lowest voltage $V_{B,W}$, for now on *Weak* cell, receives energy from the higher voltage cells $V_{B,S}$, henceforth *Strong* cells.

$$\begin{array}{ll} V_{B,W}<V_{B,i}, & I_{B,W}>0 \ \text{ receive energy} \\ V_{B,S}>V_{B,W}, & I_{B,S}<0 \ \text{ give energy} \end{array} \qquad (8)$$

During the ideal current modelling, the balancing current $I_{B,i}$of each single series connected cell will be defined under a voltage unbalanced condition, with one *Weak* cell and *(n-1) Strong* cells.

The maximum D_{cri}will be defined respect to the *Weak* cell voltage $V_{B,W}$ and the *Strong* cell voltages $V_{B,S}$. All cells that are not considered *Weak* are considered *Strong* cells.

The battery pack voltage V_{PACK} is defined as the sum of each single cell voltage $V_{B,i}$, or the sum of the *Weak* cell voltage $V_{B,W}$ with the Strong cell voltages $V_{B,S}$.

TABLE I
CHARACTERISTICS OF THE MAIN SINGLE SWITCH ACTIVE BALANCING SYSTEMS: NUMBER OF COMPONENTS AND BALANCING BEHAVIOR

Topology	S	D	C	L	T	Selective
FLY_1PnS	1	n	_	_	1	Yes
FLY_nPnSP	1	n	_	_	n	Yes
FLY_nPnSS	1	n	_	_	n	No
SEPIC	1	n	n	n+1	_	Yes
ZETA	1	n	n	n+1	_	Yes
Isolated_CUK	1	n	n+1	n+1	1	Yes

$$V_{PACK}=\sum_{i=1}^{n}V_{B,i}=V_{B,W}+\sum_{i=1}^{n-1}V_{B,Si} \qquad (9)$$

During a complete switching period the generalized equations that determine the mean AV and the root mean square values of the switching variables are expressed by

$$\begin{array}{l} X_{AV_T}=\sum_{i=1}^{n}X_{AV_i}D_i=X_{AV_1}D_1+X_{AV_2}D_2+...+X_{AV_n}D_n \\ X_{RMS_T}=\sqrt{\sum_{i=1}^{n}X_{RMS_i}{}^2D_i}=\sqrt{X_{RMS_1}{}^2D_1+X_{RMS_2}{}^2D_2+...+X_{RMS_n}{}^2D_n} \end{array} \qquad (10)$$

The topologies under study are 3 flyback based topologies and 3 buck-boost. The main parameters of these topologies regarding number of components and balancing behaviorare presented in Table I.

FLY_1PnS

The *FLY_1PnS* is a flyback converter of 1 primary and *n*secondaries wounded in the same magnetic core. The main advantage is that a single core is used to balance all the cells. The main disadvantages are that is not modular and deviations occur due to differences between windings. Good transformer design, by coaxial windings [47] or the use of commercial multiwinding transformers is necessary to avoid deviation between windings.

The energy is inserted during T_{ON} to the primary inductor L and after that the *Weak* cell secondary is polarized, inserting all the energy to the *Weak* cell during T_{OFF1}. T_{OFF2} guarantees de DCM. The *Strong* cells only give energy during the T_{ON} time because

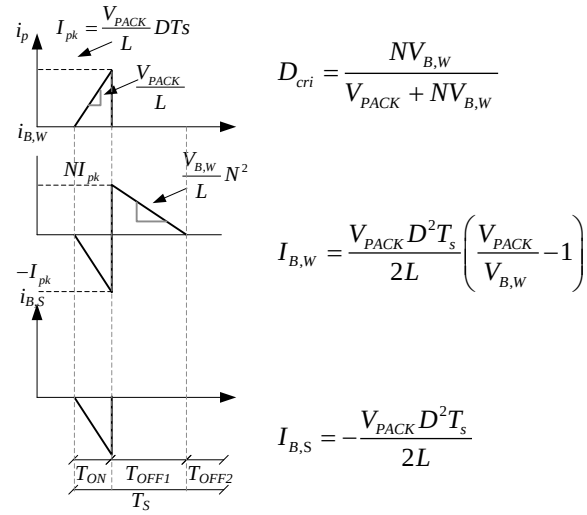

Fig. 1*FLY_1PnS* main balancing current waveforms and equations.

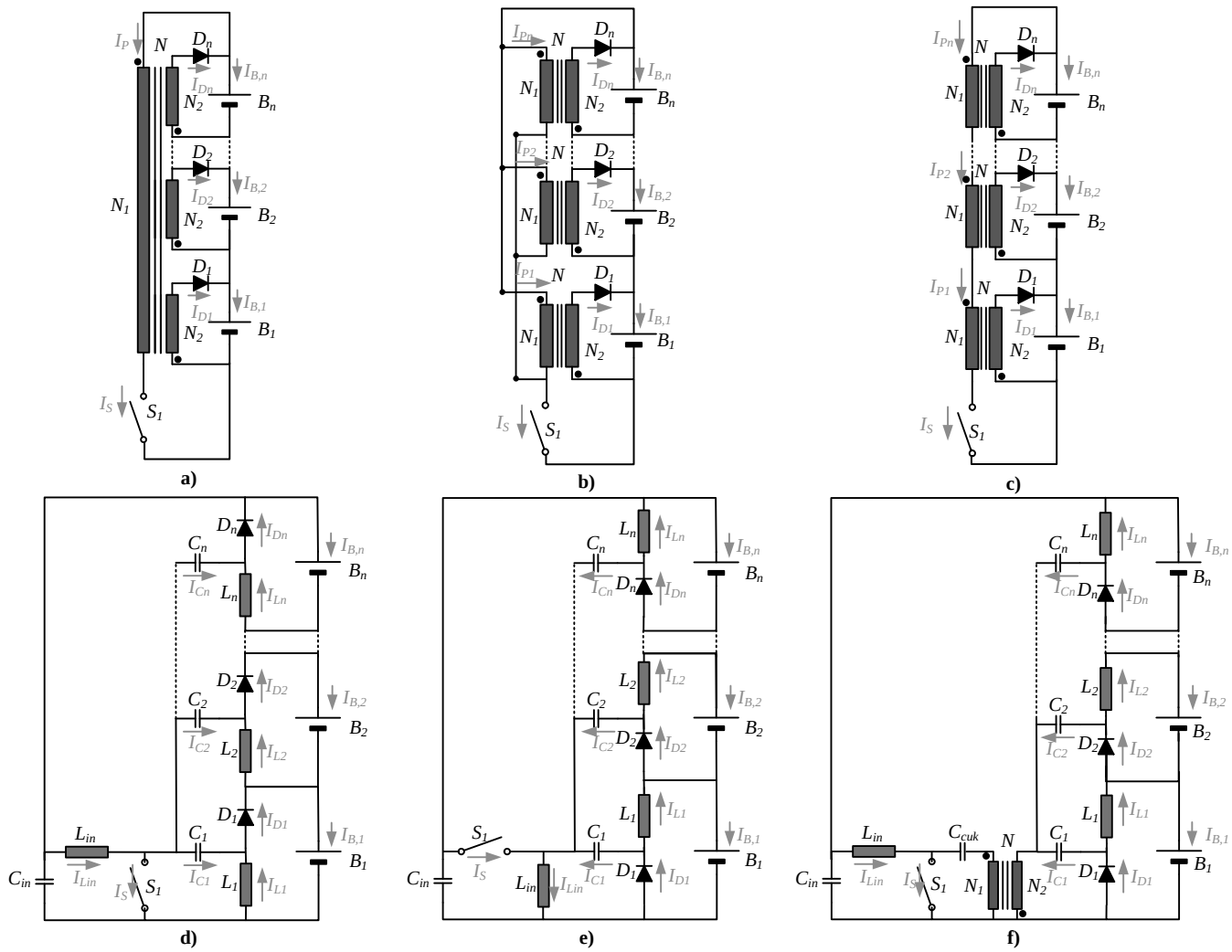

Fig. 3. Main single switch active balancing topologies schematics. a) Flyback with 1 primary and *n*secondaries with single core *FLY_1PnS* b) Flyback with *n* primaries and *n*secondaries with the primaries connected in parallel *FLY_nPnSP*. c) Flyback with *n* primaries and *n*secondaries with primaries connected in series *FLY_nPnSS*. d) The multistackedSepic topology *SEPIC*. e) The multistacked Zeta topology *ZETA*. f) The multistackedCuk topology in the isolated configuration*Isolated_CUK*.

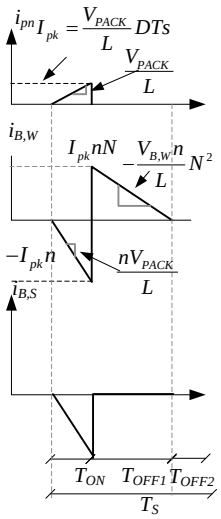

$$D_{cri} = \frac{NV_{B,W}}{V_{PACK} + NV_{B,W}} \quad (11)$$

$$I_{B,W} = \frac{V_{PACK} D^2 T_s n}{2L}\left(\frac{V_{PACK}}{V_{B,W}} - 1\right) \quad (12)$$

$$I_{B,S} = -\frac{V_{PACK} D^2 T_s n}{2L} \quad (13)$$

Fig. 2. *FLY_nPnSP*main balancing current waveforms and equations.

During Appendix the main current waveforms of the battery cells will be presented under different unbalancing effects.

FLY_nPnSP

The *FLY_nPnSP* is a flyback based design with *n* magnetic cores connected in parallel in the primary. The secondary of the *n* magnetics core is connected to each series connected cell. The main advantages are the modularity of the design and the high current capability, although it has high power losses due to high current necessity to magnetize all transformers.The current waveforms could be analyzed under different unbalancing situations inAppendix.

During T_{ON}all the magnetizing inductances L are charged with the battery pack voltage V_{PACK}inducing a big current through all the series connected cells. During T_{OFF1} the voltage of the *Weak* cell is reflected in the primary by the transformer ratio N, so all the energy stored in all the magnetizing inductors is released to the *Weak* cell.

The *Strong* cells inject energy to the circuit during T_{ON} decreasing their total energy. During T_{OFF1} there is not energy

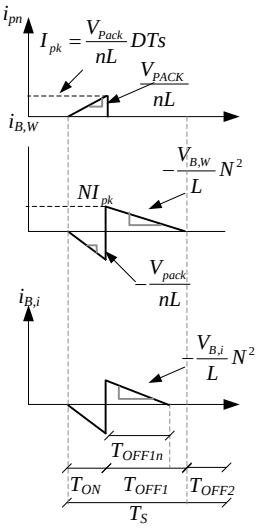

$$D_{cri} = \frac{NV_{B,W}}{\frac{V_{PACK}}{n} + NV_{B,W}} \quad (14)$$

$$I_{B,i} = \frac{V_{PACK} D^2 T_s}{2nL}\left(\frac{V_{PACK}}{nV_{B,i}} - 1\right) \quad (15)$$

Fig. 4.*FLY_nPnSS*main balancing current waveforms and equations.

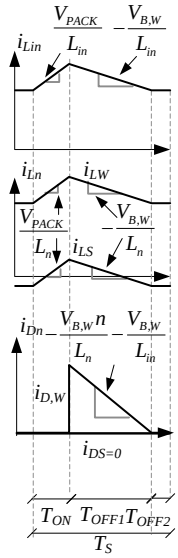

$$D_{cri} = \frac{V_{B,W}}{V_{PACK} + V_{B,W}} \quad (16)$$

$$I_{B,W} = \frac{V_{PACK} D^2 T_s \left(L_n + nL_{in}\right)}{2L_n L_{in}}\left(\frac{V_{PACK}}{V_{B,W}} - 1\right) \quad (17)$$

$$I_{B,S} = -\frac{V_{PACK} D^2 T_s \left(L_n + nL_{in}\right)}{2L_n L_{in}} \quad (18)$$

Fig. 5.*SEPIC*main balancing current waveforms and equations.

insertion to the Strong cells, so they only suffer energy decrease during T_{ON} balancing the total series connected system.

FLY_nPnSS

The flyback converter*FLY_nPnSS* is a series connection of *n* magnetic cores. The transformers are serialized and all magnetized by the same current from the battery pack. The main advantage is the modularity, but the most important drawback is the non-selective behavior.

The magnetizing inductors *L* of each transformer are charged during T_{ON}. During T_{OFF1}, the energy introduced to each transformer, is inserted back to each cell with a variable T_{OFF1} time depending on each cell Voltage $V_{B,i}$.

The *Weak* cell will have the biggest T_{OFF1} time so it will receive the biggest amount of charge, performing the balancing procedure. In the other hand, the biggest voltage cell or the strong cell, will have the smallest T_{OFF1}, receiving less energy than the energy supplies by itself.

Although each cell will have its T_{OFF1} time, the critical duty cycle D_{cri} must be guaranteed for the *Weak* cell voltage $V_{B,W}$.

SEPIC

The multistacked based Sepic converter *SEPIC* is a Sepic converter topology with *n* outputs stacked in series. The analysis of the balancing current $I_{B,i}$is not obvious so the different waveforms for different balancing situations will be presented in Appendix. The balancing current shape is dependent on the situation of each cell in the series connected string. The current ripple of the current is always bigger in the bottom connected cell.

For the analysis of the mean balancing current $I_{B,i}$, is easier to analyze the circuit in a steady state situation. The capacitor charge balance gives I_{Ci}=0, and I_{Di}=I_{Li}. The only diode that conducts is the *Weak* cell diode so $I_{D,S}$=0. Finally using Kirchhoff's current law we can determine that the balancing current $I_{B,i}$is

$$I_{B,i} = I_{D,i} - I_{Lin} \quad (19)$$

During T_{ON} all the inductors L_i and L_{in} are charged, but during T_{OFF1} only the diode of the *Weak* is polarized inserting all the energy to the *Weak* cell.

The main advantages are the transformer free solution and an easy modularity. The disadvantage is the different instantaneous current through the different series connected cells.

ZETA

The *ZETA* is also a multistacked based buck-boost topology. It has the same advantages and disadvantages of the *SEPIC* converter. The instantaneous currents are also different depending on the cell position of the series connected stack. The balancing current ripple is bigger in the top connected cell. The instantaneous currents can also be found in Appendix. Another disadvantage is also the high side switch of the topology.

The balancing current is defined as the *SEPIC* converter in (22), and the analysis of the current in steady state is equal. During T_{ON}*L,i* and *Lin* are charged and during T_{OFF1} the *Weak*

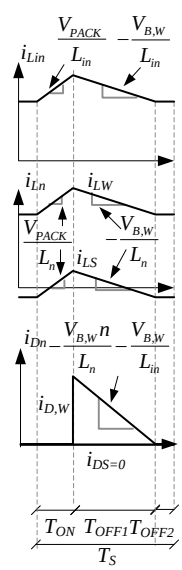

$$D_{cri} = \frac{V_{B,W}}{V_{PACK} + V_{B,W}} \quad (20)$$

$$I_{B,W} = \frac{V_{PACK} D^2 T_s \left(L_n + nL_{in}\right)}{2L_n L_{in}}\left(\frac{V_{PACK}}{V_{B,W}} - 1\right) \quad (21)$$

$$I_{B,S} = -\frac{V_{PACK} D^2 T_s \left(L_n + nL_{in}\right)}{2L_n L_{in}} \quad (22)$$

Fig. 6.*ZETA*main balancing current waveforms and equations.

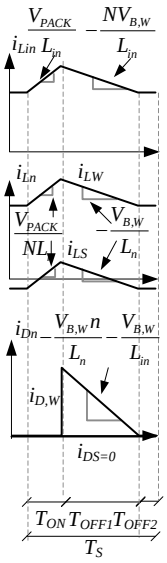

$$D_{cri} = \frac{NV_{B,W}}{V_{PACK} + NV_{B,W}} \quad (23)$$

$$I_{B,W} = \frac{V_{PACK} D^2 T_s \left(L_n + \frac{nL_{in}}{N^2} \right)}{2N^2 L_n L_{in}} \left(\frac{V_{PACK}}{V_{B,W}} - 1 \right) \quad (24)$$

$$I_{B,S} = -\frac{V_{PACK} D^2 T_s \left(L_n + \frac{nL_{in}}{N^2} \right)}{2N^2 L_n L_{in}} \quad (25)$$

Fig. 7*Isolated_CUK*main balancing current waveforms and equations.

cell diode is only polarized for $I_{B,W}$.

Isolated_CUK

The *Isolated_CUK* topology is a multistacked topology based on the Cuk converter in its isolated configuration to reverse the polarity.

The balancing current $I_{B,i}$is calculated in the steady state situation with (22). The instantaneous currents for different unbalancing situations are presented in Appendix. The current ripple is bigger in the bottom connected cell, however the current ripple in the *Isolated_CUK* is smaller than in the *SEPIC* and *ZETA* buck-boost topologies.

The biggest advantage of the *Isolated_CUK* is the modularity and the degree of freedom given by the transformer ratio *N*, to determine D_{cri}.The disadvantages are the requirement of extra components as the transformer and the split capacitor C_{cuk}.

During T_{ON} the inductors are charged and during T_{OFF1} the inductors are discharged to the *Weak* cell.

Power losses and efficiency modelling

Active balancing systems have higher efficiency than passive systems; they transfer charge between cells instead of burning the energy in a power resistor. However the efficiency of these systems is not 100% and a piece of the energy transfer of the ideal modelling is wasted in power losses.

Due to this power loss the energy transfer is reduced, and has to be taken into account. Due to DCM operation of the single switch balancing systems the efficiency modelling is harder than in CCM because

$$\begin{aligned} I_{AV} &\approx I_{RMS} \rightarrow \text{CCM} \\ I_{AV} &\neq I_{RMS} \rightarrow \text{DCM} \end{aligned} \quad (26)$$

And each component RMS current should be calculated to correctly determine the power losses and efficiency. The efficiency and power losses are dependent on the working point and the parameters of the converter.

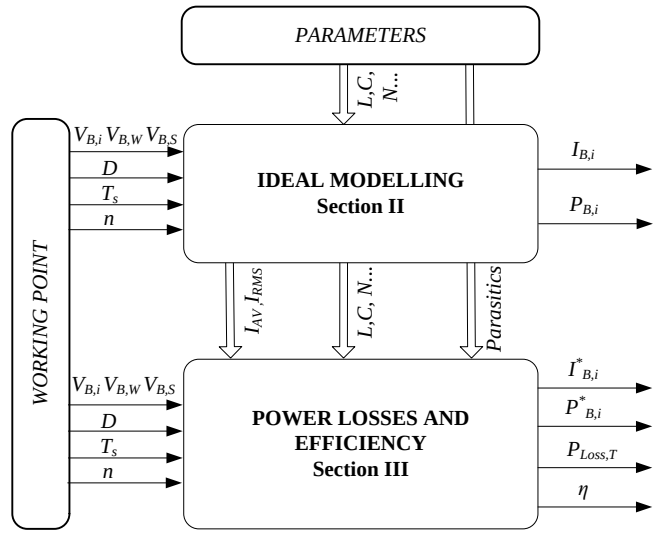

Fig. 8 Current balancing modelling strategy, with an ideal power loss modelling and an adjustment based on efficiency and power losses calculation.

The working point are the series connected cell voltages$V_{B,i}$or *Weak* and *Strong* cell voltages, the number of cells *n*, the dutycycle ratio *D*and the switching period T_s.

The parameters of the converter are the value of each passive component (*L*,*C*, *N*...) and the parasitic (R_L,*ESR*,R_{DSON},V_D,R_D…). The parasitics are only used for the efficiency and power loss calculations.

Under an unbalancing situation, the ideal balancing power of the cells $P_{,B,I}$is given by the ideal modelling currents of Section II by

$$P_{B,i} = V_{B,i} I_{B,i} \quad (27)$$

The total balancing power is defined by the sum of the module of each balancing power.

$$P_{B,T} = \sum_{i=1}^{n} \left| P_{B,i} \right| \quad (28)$$

The power losses of the converter $P_{Loss,T}$are calculated with the RMS and AV currents of each component. Switching losses are neglected due to low impact in DCM mode.

The real balancing power$P^*_{B,T}$managed by the balancing system, is then smaller than the ideal balancing power.

$$P^*_{B,T} = P_{B,T} - P_{Loss,T} \quad (29)$$

The efficiency η analysis is not obvious because a balancing system is not a typical input-output system. The cells act as both input and output sources, so the efficiency will be analyzed respect to the maximum ideal power as

$$\eta = \frac{P^*_{B,T}}{P_{B,T}} \cdot 100 = \frac{P_{B,T} - P_{Loss,T}}{P_{B,T}} \cdot 100 \Bigg\} \; unbalanced \quad (30)$$

The power losses $P_{Loss,T}$ are mainly due to the high balancing current redirected to the weak cell $I^*_{B,W}$. To recalculate the real balancing currents $I^*_{B,i}$ the power $P_{Loss,T}$ is only subtracted to the balancing power of the Weak cell, so

$$P_{Loss,T} \xrightarrow{affect} I^*_{B,W}$$
$$I^*_{B,W} = \frac{V_{B,W} I_{B,W} - P_{Loss,T}}{V_{B,W}} \qquad (31)$$
$$I^*_{B,S} = \frac{V_{B,S} I_{B,S}}{V_{B,S}} = I_{B,S}$$

For the non-selective case of the *FLY_nPnSS* the power losses are distributed to all the cells. The lowest voltage cell has bigger power losses that the *Strong* cells. The power losses $P_{Loss,T}$are distributed inversely to the voltage of the cells as

$$P_{Loss,T} \xrightarrow{FLY_nPnSS} I^*_{B,i} \text{ redistributed to all cells}$$

$$I^*_{B,i} = \frac{V_{B,i} I_{B,i} - \dfrac{P_{Loss,T} \sum_{\substack{j=1 \\ j \neq i}}^{n} V_{B,j}}{V_{PACK}}}{V_{B,i}} \qquad (32)$$

For a balanced situation the equations are different because the ideal balancing power $P_{B,i}$=0, because there is not balancing current in a balanced situation (4).

However in the real situation there is a small balancing power to compensate the power losses of the converter.

The real balancing power of the balancing system $P^*_{B,T}$is only used to compensate the power losses, so the efficiency of the converter is 0 because it does not transfer any energy. The efficiency equation is different for balanced and unbalanced situation.

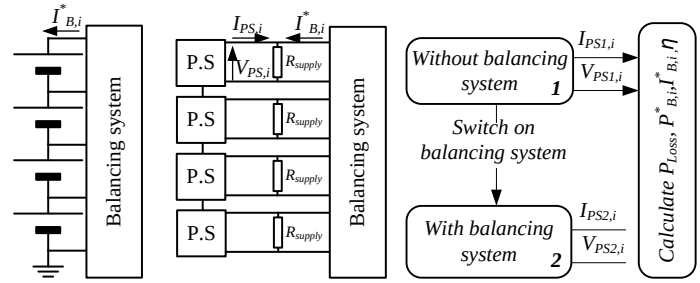

a) **b)** **c)**

Fig. 9 Balancing system connection for a 4S1P configuration. a) Real battery test configuration. b) Simulated test bench configuration. C) Flow chart for power and efficiency measurements with direct power supply measurement.

$$\left.\begin{aligned} &P_{B,T} = 0 \\ &P^*_{B,T} \approx P_{Loss,T} \\ &\eta = \frac{P^*_{B,T} - P_{Loss,T}}{P^*_{B,T}} \cdot 100 \approx 0 \end{aligned}\right\} \text{balanced} \qquad (33)$$

Experimental results

To evaluate the ideal modelling and the power loss and efficiency models presented in Section II and Section III the 6 balancing systems under study have been designed to evaluate mod elling equations.

1. Table II
2. Design and Ideal Prototype parameters for a working point of one *Weak* cell $V_{B,W}$=2 V and 3 *Strong* cells $V_{B,S}$=3.65 V for 4S1P battery pack n=4 switching period T_s=10 µs

	3. Design					4.	5. Prototype				
Topology	6. $I_{B,W}$ [mA]	7. 8. D []	9. L_n [µH]	10. L_{in}[µH]	11. 12. N []	13.	14. $I_{B,W}$ [mA]	15. 16. D []	17. L_n [µH]	18. L_{in}[µH]	19. 20. N []
FLY_1P4S	400	0.134	16	_	1		500	0.13	12	_	1
FLY_4P4SP	400	0.134	63	_	1		600	0.13	40	_	1
FLY_4P4SS	100	0.382	15	_	1		144	0.38	10	_	1
SEPIC	400	0.134	66	427	_		365	0.13	68	470	_
ZETA	400	0.134	66	427	_		365	0.13	68	470	_
Isolated_CUK	400	0.134	66	427	1		365	0.13	68	470	1

The balancing converters are designed for a 4S1P 6.5 Ah $LiFePO_4$ battery pack, so the series connected cell umber is n=4. The maximum cell voltage of $LiFePO_4$ cells is 3.65 V and the minimum cell voltage is 2 V. The converter is designed to inject to the *Weak* cell a fixed balancing current $I_{B,W}$under the biggest unbalancing situation, with the *Weak* cell voltage$V_{B,W}$ at 2V and the rest 3 *Strong* cells $V_{B,S}$at maximum 3.65 V. The battery pack voltage for that unbalancing situation is defined by (6) to V_{PACK}= 12.95 V.

The switching frequency F_s has been defined to 100 kHz, so the switching period T_s is 10 µs. The Weak cell balancing current $I_{B,W}$ was defined as 400 mA, except for the *FLY_4P4SS* which was defined as 100 mA. The parameters to meet these characteristics are defined in Table II. The differences between the designed converter and the real prototypes respect to ideal current modelling are presented.

Forthe flyback topologies when defined as $L_n$in Table IIis referred to the magnetizing inductance L. For the magnetic components WürthElektronik devices are used. The transformers are 1:1 relation WE-DD series Power Chokes. The inductors are WE-PD3 SMD Shielded Power Inductors.

The capacitors for the charge transfer of the buck boost topologies are Kemet SMD MLCCs withC_n= 10µF. The high capacitance value is defined to guarantee a constant voltage during the whole switching period in the capacitor.

The *isolated_CUK* converter isolation is made by a WE-DD 47 µH magnetizing inductor 1:1 transformer and the capacitor split C_{CUK} =10 µF.

The diodes D_n are low voltage drop Vishay SL13-E3/61T – Schottky rectifiers. Schottky diodes reduce power losses in low voltage applications.

The low R_{DSON} "Power Trench" FDS6682 N-Channel Mosfet of Fairchild Semiconductor have been used as the single switch for the 6 different topologies.

The duty cycle D is fixed. The DCM is guaranteed for all the operating points because the critical duty cycle D_{cri} is calculated for the biggest unbalancing situation.

To switch the power converter in an open loop configuration a GW INSTEK AFG-2005Arbitary Function Generator has been used. This function Generator gives the versatility of full duty cycle control, 0.01 to 0.99, for a 100 kHz base frequency.

To prove the balancing behavior of the single switch balancing systems an experimental test bench has been designed. The experimental test bench consists of one power supply and a parallel connected resistorR_{supply} simulating a single battery cell. The parallel connection of the power supply and the power resistor permits to simulate the two quadrant behavior of a single battery cell. The power supply gives energy when simulating a *Strong* cell and the resistor absorbs current when current is injected to the *Weak* cell. The power capability of theR_{supply} has to be high enough to absorb all the energy delivered by the balancing system.

To simulate the 4 series connected single cells 2 high performance HamegHM7042-5 power supplies are used. Each power supply has 2 independent voltage outputs where a 3.3 Ω high power R_{supply} is connected in parallel. After that the simulated battery cells are connected in series to simulate a 4S1P battery pack.

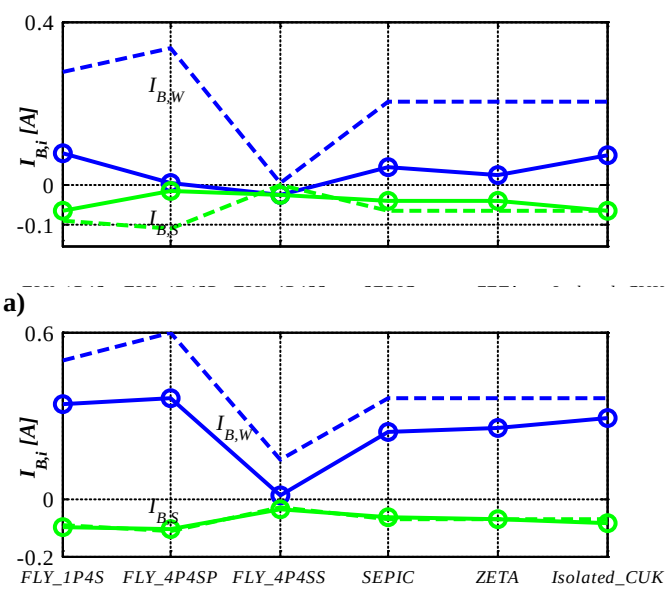

a)

b)

Fig. 10.*Weak* cell balancing current $I_{B,W}$ and *Strong* cell balancing current $I^*_{B,S}$ under an unbalancing situation. Dashed (--) ideal balancing currents $I_{B,i}$ and filled-circle(o) real balancing currents $I^*_{B,i}$ a) Small unbalance $V_{B,W}$=3.1 V $V_{B,S=}$3.2 V b) Big unbalance: $V_{B,W=}$2 V and $V_{B,S=}$3.65.

The Hameg HM7042-5 permits to read directly the currentI_{PS} with 1 mA resolution and the voltageV_{PS} with 10 mV resolution. The good resolution permits to obtain accurate power measurements directly from the power supply.

To measure the main parameters of the converter the flow chart of Fig. 9 c) is presented which is divided in two steps

First step (step 1) measures the current $I_{PS1,i}$and the power $P_{PS1,i}$of each power supply with the resistors connected, the balancing system connected, but the balancing system switched off. During step 1 the power supply will only power the resistors.

During step 2 the balancing system is switched on. The voltage$V_{PS2,i}$ and the current $I_{PS2,i}$of each power supply is measured. The power supplies continue to injecting the same power to the resistors, but the power losses of the converter are also supplied. The balancing system should give current to the less voltage resistor, decreasing the current contribution from the less voltage power supply, and increasing the current contributed from the high voltage power supplies.

During step 1 and step 2 the current fed to the resistor is equal because the voltage does not change. The change in the supply current is due to the balancing process of the balancing system. During step 1 $I^*_{B,i}$=0, so the real balancing current $I^*_{B,i}$could be easily measured by the difference between the supply current in step 1 and the supply current in step 2.

$$I^*_{B,i} = I_{PS1,i} - I_{PS2,i} \tag{34}$$

The balancing power $P^*_{B,i}$ is then defined by the balancing current and the power supply voltage, the total balancing power $P^*_{B,T}$ is defined in the same way as in(28).

$$P^*_{B,i} = V_{B,i} I^*_{B,i} = V_{PS,i} I^*_{B,i} \qquad P^*_{B,T} = \sum_{i=1}^{4} \left| P^*_{B,i} \right| \tag{35}$$

During step 1 the only power consumption are the R_{supply} resistors. When the active balancing converter is connected we have the R_{supply} losses and the total power loss of the converter $P_{Loss,T}$. The power ofstep 2 minus the power of step 1 are the converter total power losses P_{LossT}

$$P_{Loss,T} = \sum_{i=1}^{4} V_{PS2,i} I_{PS2,i} - \sum_{i=1}^{4} V_{PS1,i} I_{PS1,i} \tag{36}$$

The efficiency of the balancing system η is them calculated as

$$\eta = \frac{P^*_{B,T}}{P^*_{B,T} + P_{Loss}} \tag{37}$$

Behavior under unbalancing situation

The first experimental step is to verify the correct behavior of the 6 single switch unbalancing systems under unbalancing situation. For that issue the test bench will be configured under two different unbalancing situations.

The first unbalancing situation will be a small unbalance between cells. The *Weak* cell simulated Power Supply will be established at $V_{B,W}$=3.1 V and the *Strong* cell voltages to $V_{B,S}$=3.2 V.

The second unbalancing situation will be a big unbalance. The *Weak* cell voltage is $V_{B,W}$=2 V and the strong cell voltages will be established to the maximum cell voltages of the $LiFePO_4$ cells $V_{B,S}$=3.65 V.

Fig. 10presents the balancing currents under different situation with the ideal design values under dashed lines (--) and

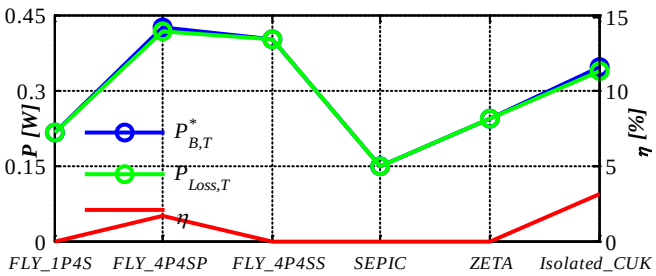

Fig. 11. Total real balancing power $P^*_{B,T}$and power losses $P_{Loss,T}$ under a balanced situation with $V_{B,i}$=3.65V. Maximum power losses occur at maximum cell voltage. Efficiency $\eta$is calculated under balanced situation equation presented in (33).

the real application currents in filled circles (o). The ideal balancing current is bigger than the real balancing current.

During small unbalance and big unbalance the *Weak* cell balancing current $I_{B,W}$is always higher than the *Strong* cell balancing current$I_{B,S}$. A natural balancing process occurs between Strong cells and the Weak cell.

The non-selective*FLY_4P4SS* converter gives the smallest difference between the *Weak* cell balancing current and the strong cell current. This topology will not be suitable when big balancing power is required to balance the cells in a short period of time.

The primary parallel connected *FLY_4P4SP* gives big balancing current under big unbalancing situations Fig. 10 b)., however in small unbalancing conditions Fig. 10 a), the high power losses reduce the balancing power of the converter.

Behavior under balanced situation

During balanced situation the power losses and the balancing power are nearly equal as presented in (30).

The balanced situation is generated with $V_{B,i}$= 3.65 V to generate the maximum power losses.

Fig. 11presents the difference between the real balancing power $P^*_{B,T}$and the total power losses$P_{Loss,T}$. It is demonstrated that the balancing power only exchanges power to meet the power losses requirement.

Regarding to (33) is clearly seen that the efficiency η is nearly 0. Little differences appear in the *FLY_4P4SP* and the *Isolated_CUK* due to non-idealities, but they have not big impact.

Model and experimental comparison

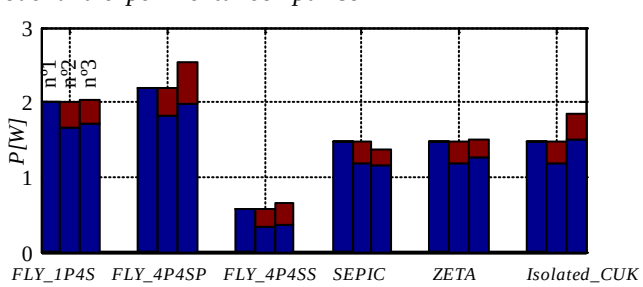

Fig. 12. Total balancing power $P_{B,T}$and power losses $P_{Loss,T}$ comparison for each balancing system. Bar nº1 ideal balancing model. Bar nº2 power losses model. Bar nº3 real experimental results. Red bar: Power losses $P_{Loss,T}$ and blue Bar total balancing power $P_{B,T}$

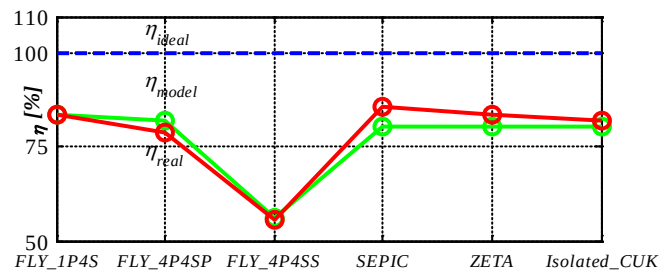

Fig. 13. Ideal balancing efficiency η_{ideal}, modelled efficiency η_{model} and the real experimental efficiency η_{real}, for all the 6 different balancing systems under a big unbalance situation $V_{B,W}$=2 V and $V_{B,S}$=3.65 V.

Experimental results and model equations are going to be compared under an unbalancing situation. Main parameters and results are resumed in Table III.

The unbalancing is performed between a *Weak* cell voltage $V_{B,W}$=2 V and the strong cell voltages $V_{B,S}$=3.65 V.

First the power losses $P_{loss,T}$and the total balancing power $P_{B,T}$will be compared between the ideal modelling, the modelling with the power losses taken into account and the real experimental results.

Fig. 15 presents the comparison between the ideal balancing design (Bar nº1), the parasitic modelled design (Bar nº2) and the real experimental results (Bar nº3). The red part of the bar are the power losses $P_{loss,T}$and the blue part is the total balancing power $P_{B,T}$.

The ideal balancing model represented in the first Bar (Bar nº1) injects the maximum energy to the system, without any power loss.

The power losses model presented in section III and represented in Fig. 12 by Bar nº2, give the new balancing power $P^*_{B,T}$when the power losses of the converter are taken into account.

Bar nº3 of Fig. 12 give the power measurements made by the direct measurements of the power supply.

Good accuracy between real results and power losses is expected, knowing that power losses measurement in low power devices and high switching frequency devices is a difficult job.

The efficiency ηdecreases respected to the 100 % ideal efficiency. A good approach between experimental and modelled is obtained thanks to the RMS calculations of DCM currents.

For the selective balancing systems is kept around 75 %Fig. 13.

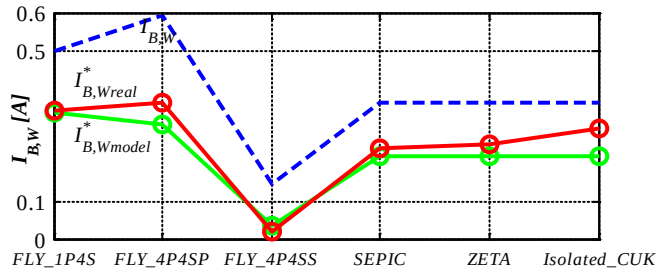

Fig. 14. Ideal *Weak* balancing current $I_{B,W}$in dashed blue. Modelld real *Weak* balancing current $I^*_{B,W}$filled circle green. Real experimental *Weak* balancing current $I^*_{B,W}$filled red circle.

21. Table III
22. Ideal, modelled and real data comparison. Total balancing power $P_{B,T}$, Total power losses $P_{Loss,T}$, efficiency η and balancing current of the *Weak* cell $I_{B,W}$. Working point unbalanced $V_{B,W}$=2 V and $V_{B,S}$=3.65 V.

	23. $P_{B,T}$ [W]			24. 25. $P_{Loss,T}$[W]			26. 27. η [%]			28. 29. $I_{B,W}$[A]		
	30. Ideal	31. Model	*32. Real*	*33. 34. Ideal*	*35. Model*	*36. Real*	*37. 38. Ideal*	*39. Model*	*40. Real*	*41. 42. Ideal*	*43. Model*	*44. Real*
FLY_1P4S	1.997	1.672	1.708	0	0.325	0.328	100	83.71	83.88	0.499	0.337	0.345
FLY_4P4SP	2.198	1.809	1.991	0	0.388	0.535	100	82.33	78.82	0.599	0.305	0.364
FLY_4P4SS	0.578	0.324	0.366	0	0.254	0.29	100	56.05	55.78	0.145	0.037	0.02
SEPIC	1.461	1.175	1.163	0	0.286	0.195	100	80.43	85.64	0.365	0.222	0.242
ZETA	1.461	1.175	1.256	0	0.286	0.245	100	80.43	83.81	0.365	0.222	0.254
Isolated_CUK	1.461	1.174	1.508	0	0.286	0.332	100	80.4	81.96	0.365	0.222	0.294

The biggest the unbalancing is, the higher the efficiency reached by the balancing system.

The non-selective balancing system*FLY_4P4SS* has the lowest efficiency nearly 50% because produces high power losses due to the current flow to all the series connected cells. The efficiency is low even if the balancing current of the system is the lowest.

With the power losses modelling and the efficiency calculation a new estimation of the real balancing current $I^*_{B,i}$ could be made. The power losses are subtracted to the *Weak* cell (31) except for the non-selective *FLY_4P4SS* converter that are redistributed inversely proportional to the voltage as presented in (32).

The balancing current is reduced due to the power losses of the converter Fig. 14. The modelled *Weak* cell balancing current $I^*_{B,Wmodel}$ permits to evaluate the real balancing current, with good accuracy.

II. Conclusions

During this present work main single switch active balancing topologies have been analyzed, modelled and tested.

Single switch active balancing systems present high simplicity due to a unique active device is used. They also have the natural behavior to balance series connected cells with an open loop control strategy. For that issue, DCM mode must be guaranteed during all the working points.

During Section II the ideal balancing behavior and equations are presented for the 6 most representative singe switch balancing systems. The ideal modelling is focused on the energy transfer between the *Strong* cells and the *Weak* cell of a series connected energy storage system. The maximum critical duty cycle equation D_{cri} is defined, and the balancing currents of the *Weak* cell $I_{B,W}$and the strong cells $I_{B,S}$are defined. The Ideal modelling equations give the main parameters for the design of a single switch active balancing system because the energy transfer between the *Weak* cells and the *Strong* cells is defined.

Section III presents the power loss modelling of the single switch balancing systems. The power losses $P_{Loss,T}$of the converters are taken into account to measure the power reduction of the converter. Due to DCM operation the RMS and AV currents of all the components should be modelled to correctly estimate the power losses $P_{Loss,T}$. This approach gives a most accurate model of the balancing currents $I^*_{B,i}$and the converter balancing power $P^*_{B,T}$.

For the experimental results presented in Section IV the 6 different balancing systems have been designed and constructed to compare different behaviors under unbalanced and balanced situations. A power supply based test bench has been designed to simulate series connected cells unbalances and measure the power losses $P_{Loss,T}$and balancing power $P^*_{B,T}$indirectly by the power supply measurements. Duringunbalancing situation it has been seen that the *Weak* cell balancing current $I^*_{B,W}$is always bigger that the *Strong* cells balancing current $I^*_{B,S}$. During balanced situation it has been demonstrated that the balancing power of the system only contributes energy to compensate the power losses of the system. No energy is exchanged between the cells. Ideal, modelled and experimental results are compared to evaluate the accuracy of the modelling and main conclusions are obtained.

The balancing system efficiency η for a big unbalance case is kept above 75%. It is a high efficiency for systems which manage only 2 Watts of balancing power.

The non-selective *FLY_4P4SS* is the lowest efficiency system, and is not selective, decreasing the balancing speed of the system. This topology is the worst located for future balancing system designs.

Between the selective topologies, the efficiencies are similar and the behavior is similar. The *FLY_4P4SP* with the primaries in parallel has the worst behavior when a small balance is produced, due to higher power losses.

The*Isolated_CUK* will be a good balancing system candidate when high numbers of cells are connected in series. When high number of cells are connected in series the D_{cri} could be very small, and the degree of freedom of the transformer ratio gives flexibility in the value of the duty cycle. This also happens in the different flyback topologies.

Futurework

Future work will be held by testing the balancing systems in real battery pack tests. The main results of the energy increase and voltage balancing effect will be presented in future publications.

Appendix

The Appendix presents main single switch topologies current waveforms for two different unbalancing situations for a 4S1P battery back. The unbalancing effect will be analyzed by inserting a weak cell in the bottom cell or first cell (Scenario 1) or in the second cell (Scenario 2).

During Appendix it will be presented that is independent that the *Weak* cell is in the bottom or in the top part of the series connected cells.

The characteristics balancing currents presented in Fig. 15are presented with the prototype parameters presented in Table II. The DCM operation is guaranteed for both unbalancing scenarios presented in Table IV. This case is guaranteed because D=0.13, the critical duty cycle for a balancing situation of $V_{B,W}$= 2 V and $V_{B,S}$=3.65 V.

Non-selective behavior of the *FLY_4P4SS* balancing system is clearly observed. During T_{OFF1} period the balancing current flows to all the cells, not only to the *Weak* cell.

The *FLY_1P4S* and the *FLY_4P4SP* are selective topologies as could be seen in Fig. 15. It is also presented the higher peak current managed by the *FLY_4P4SP* due to the parallel operation of the balancing system.

The buck- boost based topologies have different behavior regarding current ripple depending the situation of the cell in the series connected string.

45. Table IV
46. Different unbalancing scenarios For single switch balancing system current analysis

Scenario	47. $V_{B,1}$	48. $V_{B,2}$	49. $V_{B,3}$	50. $V_{B,4}$
1	2	3	3	3
2	3	2	3	3

The *SEPIC* topology has bigger current ripple in the bottom cell (cell 1), the *ZETA* configuration in the top cell (cell 4) and the *Isolated_CUK* in the bottom cell (cell 1). Even the current ripple is different the mean current introduced to all the strong cells is equal.

The *Weak* cell mean current is always bigger than the *Strong* cells mean current.

The T_{OFF1} period depends directly in the *Weak* cell voltage, except for the non-selective *FLY_4P4SS*, were the biggest T_{OFF1} period is the *Weak* cell voltage current but the other cells have different T_{OFF1} periods depending on their voltages.

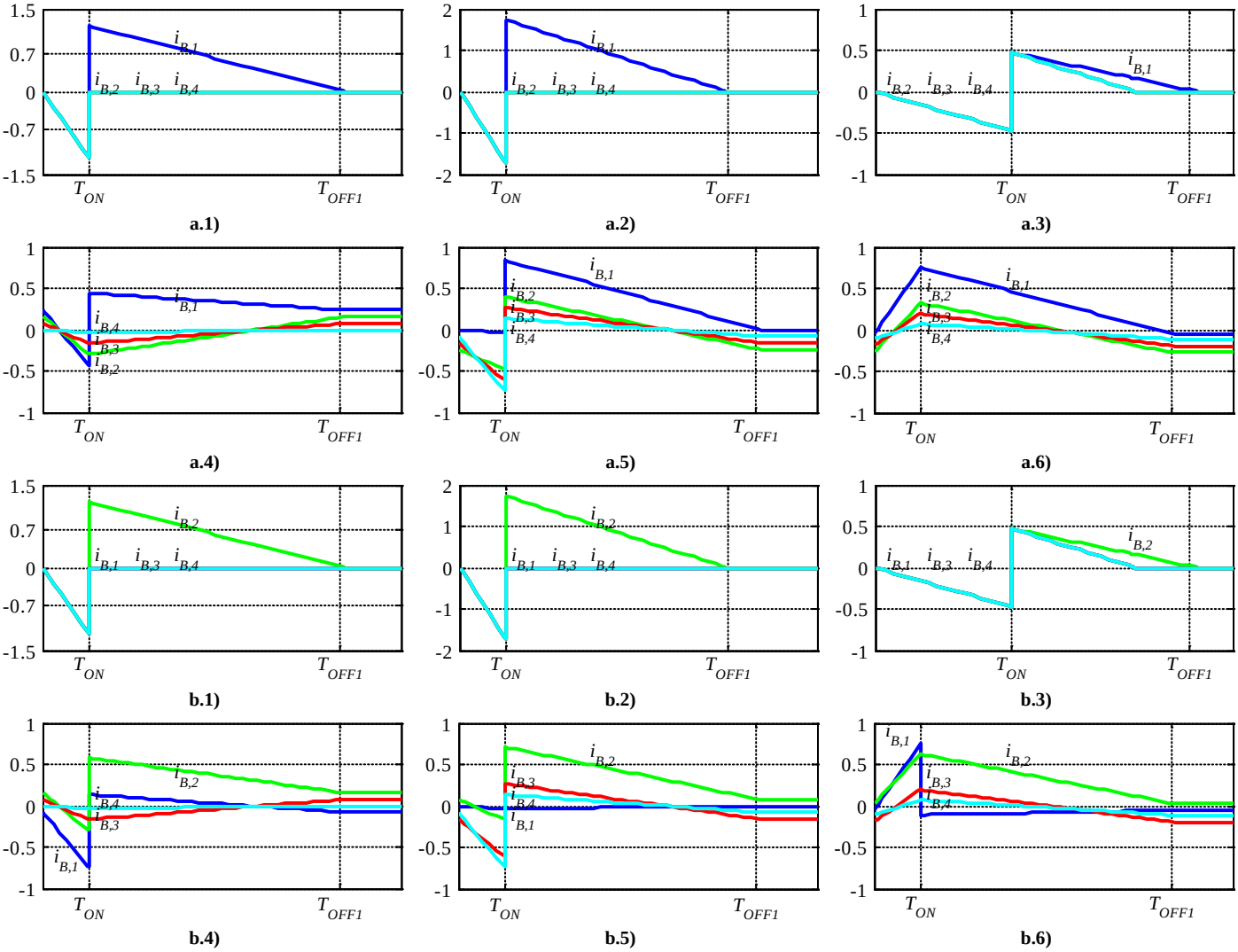

Fig. 15. Single switch balancing current waveforms. Vertical Axis: Balancing currents $I_{B,i}$ [A]. Letter index: a) Scenario1, b) Scenario 2. Number index: 1) *FLY_1P4S* 2) *FLY_4P4SP* 3) *FLY_4P4SS* 4) *SEPIC* 5) *ZETA*, 6) *Isolated_CUK*.

REFERENCES

[1] E. Comission, "Energy 2020 - A strategy for competitive, sustainable and secure energy," Brussels, 2010. .

[2] EVE, "Basque country energy strategy 2020 (E2020)," p. 236, 2012.

[3] S. Gill, I. Kockar, and G. W. Ault, "Dynamic Optimal Power Flow for Active Distribution Networks," Power Systems, IEEE Transactions on, vol. 29, no. 1. pp. 121–131, 2014.

[4] C. Abbey and G. Joos, "Supercapacitor Energy Storage for Wind Energy Applications," Industry Applications, IEEE Transactions on, vol. 43, no. 3. pp. 769–776, 2007.

[5] K. Agbossou, M. Kolhe, J. Hamelin, and T. K. Bose, "Performance of a stand-alone renewable energy system based on energy storage as hydrogen," Energy Conversion, IEEE Transactions on, vol. 19, no. 3. pp. 633–640, 2004.

[6] J. P. Barton and D. G. Infield, "Energy storage and its use with intermittent renewable energy," Energy Conversion, IEEE Transactions on, vol. 19, no. 2. pp. 441–448, 2004.

[7] B. S. Borowy and Z. M. Salameh, "Methodology for optimally sizing the combination of a battery bank and PV array in a wind/PV hybrid system," Energy Conversion, IEEE Transactions on, vol. 11, no. 2. pp. 367–375, 1996.

[8] J. M. Carrasco, L. G. Franquelo, J. T. Bialasiewicz, E. Galvan, R. C. P. Guisado, M. A. M. Prats, J. I. Leon, and N. Moreno-Alfonso, "Power-Electronic Systems for the Grid Integration of Renewable Energy Sources: A Survey," Industrial Electronics, IEEE Transactions on, vol. 53, no. 4. pp. 1002–1016, 2006.

[9] B. Hartmann and A. Dan, "Methodologies for Storage Size Determination for the Integration of Wind Power," Sustainable Energy, IEEE Transactions on, vol. 5, no. 1. pp. 182–189, 2014.

[10] N. Mendis, K. M. Muttaqi, and S. Perera, "Management of Battery-Supercapacitor Hybrid Energy Storage and Synchronous Condenser for Isolated Operation of PMSG Based Variable-Speed Wind Turbine Generating Systems," Smart Grid, IEEE Transactions on, vol. 5, no. 2. pp. 944–953, 2014.

[11] K. Strunz, E. Abbasi, and D. N. Huu, "DC Microgrid for Wind and Solar Power Integration," Emerging and Selected Topics in Power Electronics, IEEE Journal of, vol. 2, no. 1. pp. 115–126, 2014.

[12] C. X. Wu, C. Y. Chung, F. S. Wen, and D. Y. Du, "Reliability/Cost Evaluation With PEV and Wind Generation System," Sustainable Energy, IEEE Transactions on, vol. 5, no. 1. pp. 273–281, 2014.

[13] F. Diaz-Gonzalez, F. D. Bianchi, A. Sumper, and O. Gomis-Bellmunt, "Control of a Flywheel Energy Storage System for Power Smoothing in Wind Power Plants," Energy Conversion, IEEE Transactions on, vol. 29, no. 1. pp. 204–214, 2014.

[14] S. Teleke, M. E. Baran, A. Q. Huang, S. Bhattacharya, and L. Anderson, "Control Strategies for Battery Energy Storage for Wind Farm Dispatching," Energy Conversion, IEEE Transactions on, vol. 24, no. 3. pp. 725–732, 2009.

[15] G. Xu, L. Xu, D. J. Morrow, and D. Chen, "Coordinated DC Voltage Control of Wind Turbine With Embedded Energy Storage System," Energy Conversion, IEEE Transactions on, vol. 27, no. 4. pp. 1036–1045, 2012.

[16] A. F. Burke, "Batteries and Ultracapacitors for Electric, Hybrid, and Fuel Cell Vehicles," Proceedings of the IEEE, vol. 95, no. 4. pp. 806–820, 2007.

[17] A. Khaligh and Z. Li, "Battery, Ultracapacitor, Fuel Cell, and Hybrid Energy Storage Systems for Electric, Hybrid Electric, Fuel Cell, and Plug-In Hybrid Electric Vehicles: State of the Art," Vehicular Technology, IEEE Transactions on, vol. 59, no. 6. pp. 2806–2814, 2010.

[18] O. Briat, J.-M. Vinassa, W. Lajnef, S. Azzopardi, and E. Woirgard, "Principle, design and experimental validation of a flywheel-battery hybrid source for heavy-duty electric vehicles," Electric Power Applications, IET, vol. 1, no. 5. pp. 665–674, 2007.

[19] E. Schaltz, A. Khaligh, and P. O. Rasmussen, "Influence of Battery/Ultracapacitor Energy-Storage Sizing on Battery Lifetime in a Fuel Cell Hybrid Electric Vehicle," Vehicular Technology, IEEE Transactions on, vol. 58, no. 8. pp. 3882–3891, 2009.

[20] E. Tara, S. Shahidinejad, S. Filizadeh, and E. Bibeau, "Battery Storage Sizing in a Retrofitted Plug-in Hybrid Electric Vehicle," Vehicular Technology, IEEE Transactions on, vol. 59, no. 6. pp. 2786–2794, 2010.

[21] H. Yoo, S.-K. Sul, Y. Park, and J. Jeong, "System Integration and Power-Flow Management for a Series Hybrid Electric Vehicle Using Supercapacitors and Batteries," Industry Applications, IEEE Transactions on, vol. 44, no. 1. pp. 108–114, 2008.

[22] C.-S. Moo, K. S. Ng, and Y.-C. Hsieh, "Parallel Operation of Battery Power Modules," Energy Conversion, IEEE Transactions on, vol. 23, no. 2. pp. 701–707, 2008.

[23] C.-S. Moo, K.-S. Ng, and J.-S. Hu, "Operation of battery power modules with series output," Industrial Technology, 2009. ICIT 2009. IEEE International Conference on. pp. 1–6, 2009.

[24] T. Kim, W. Qiao, and L. Qu, "A series-connected self-reconfigurable multicell battery capable of safe and effective charging/discharging and balancing operations," Applied Power Electronics Conference and Exposition (APEC), 2012 Twenty-Seventh Annual IEEE. pp. 2259–2264, 2012.

[25] F. Jin and K. G. Shin, "Pack Sizing and Reconfiguration for Management of Large-Scale Batteries," Cyber-Physical Systems (ICCPS), 2012 IEEE/ACM Third International Conference on. pp. 138–147, 2012.

[26] T. Kim, W. Qiao, and L. Qu, "Power Electronics-Enabled Self-X Multicell Batteries: A Design toward Smart Batteries," Power Electronics, IEEE Transactions on, vol. PP, no. 99. p. 1, 2012.

[27] H. Qian, J. Zhang, J.-S. Lai, and W. Yu, "A High-Efficiency Grid-Tie Battery Energy Storage System," Power Electronics, IEEE Transactions on, vol. 26, no. 3. pp. 886–896, 2011.

[28] J. R. Belt, C. D. Ho, T. J. Miller, M. A. Habib, and T. Q. Duong, "The effect of temperature on capacity and power in cycled lithium ion batteries," J. Power Sources, vol. 142, no. 1–2, pp. 354–360, Mar. 2005.

[29] S. Santhanagopalan and R. E. White, "Quantifying Cell-to-Cell Variations in Lithium Ion Batteries," Int. J. Electrochem., vol. 2012, pp. 1–10, 2012.

[30] M. Uno and K. Tanaka, "Influence of High-Frequency Charge-Discharge Cycling Induced by Cell Voltage Equalizers on the Life Performance of Lithium-Ion Cells," Vehicular Technology, IEEE Transactions on, vol. 60, no. 4. pp. 1505–1515, 2011.

[31] I. Aizpuru, U. Iraola, J. M. Canales, E. Unamuno, and I. Gil, "Battery pack tests to detect unbalancing effects in series connected Li-ion cells," Clean Electrical Power (ICCEP), 2013 International Conference on. pp. 99–106, 2013.

[32] C. Martinez, "Cell Balancing Maximizes The Capacity Of Multi-Cell Li-Ion Battery Packs," Intersil. Inc.

[33] Y. Barsukov and T. Instruments, "Battery Cell Balancing : What to Balance and How."

[34] W. C. Lee, D. Drury, and P. Mellor, "Comparison of passive cell balancing and active cell balancing for automotive batteries," Vehicle Power and Propulsion Conference (VPPC), 2011 IEEE. pp. 1–7, 2011.

[35] B. Lindemark, "Individual cell voltage equalizers (ICE) for reliable battery performance," Telecommunications Energy Conference, 1991. INTELEC '91., 13th International. pp. 196–201, 1991.

[36] S. Moore, "A review of cell equalization methods for lithium ion and lithium polymer battery systems," 2001.

[37] C.-H. Kim, M. Kim, J.-H. Kim, and G.-W. Moon, "Modularized charge equalizer with intelligent switch block for lithium-ion batteries in an HEV," Telecommunications Energy Conference, 2009. INTELEC 2009. 31st International. pp. 1–6, 2009.

[38] C.-H. Kim, M.-Y. Kim, Y.-D. Kim, and G.-W. Moon, "A modularized charge equalizer using battery monitoring IC for series connected Li-Ion battery strings in an electric vehicle," Power Electronics and ECCE Asia (ICPE & ECCE), 2011 IEEE 8th International Conference on. pp. 304–309, 2011.

[39] C.-H. Kim, M.-Y. Kim, H.-S. Park, and G.-W. Moon, "A Modularized Two-Stage Charge Equalizer With Cell Selection Switches for Series-Connected Lithium-Ion Battery String in an HEV," Power Electronics, IEEE Transactions on, vol. 27, no. 8. pp. 3764–3774, 2012.

[40] C. Kim, H. Park, G. Moon, and A. C. Description, "A Modularized Two-Stage Charge Equalization Converter for Series Connected Lithium-Ion Battery Strings in an HEV," pp. 992–997, 2008.

[41] H.-S. Park, C.-E. Kim, C.-H. Kim, G.-W. Moon, and J.-H. Lee, "A Modularized Charge Equalizer for an HEV Lithium-Ion Battery String," Industrial Electronics, IEEE Transactions on, vol. 56, no. 5. pp. 1464–1476, 2009.

[42] H.-S. Kim, K.-B. Park, S.-H. Park, G.-W. Moon, and M.-J. Youn, "A new two-switch flyback battery equalizer with low voltage stress on the switches," Energy Conversion Congress and Exposition, 2009. ECCE 2009. IEEE. pp. 511–516, 2009.

[43] H.-S. Park, C.-H. Kim, K.-B. Park, G.-W. Moon, and J.-H. Lee, "Design of a Charge Equalizer Based on Battery Modularization," Vehicular Technology, IEEE Transactions on, vol. 58, no. 7. pp. 3216–3223, 2009.

[44] J. Ewanchuk, D. Yague, and J. Salmon, "A modular balancing bridge for series connected Li-ion batteries," Energy Conversion Congress and Exposition (ECCE), 2011 IEEE. pp. 2908–2915, 2011.

[45] M. Uno and K. Tanaka, "Single-Switch Cell Voltage Equalizer Using Multistacked Buck-Boost Converters Operating in Discontinuous Conduction Mode for Series-Connected Energy Storage Cells," Vehicular Technology, IEEE Transactions on, vol. 60, no. 8. pp. 3635–3645, 2011.

[46] M. Uno and K. Tanaka, "Single-Switch Multi-Output Charger Using Voltage Multiplier for Series-Connected Lithium-Ion Battery/Supercapacitor Equalization," Industrial Electronics, IEEE Transactions on, vol. PP, no. 99. p. 1, 2012.

[47] N. H. Kutkut, H. L. N. Wiegman, D. M. Divan, and D. W. Novotny, "Design considerations for charge equalization of an electric vehicle battery system," IEEE Trans. Ind. Appl., vol. 35, no. 1, pp. 28–35, 1999

AUTHORS

First Author Dr. Iosu Aizpuru. Computing and Electronics department, University of Mondragon, Arrasate- Mondragon, Spain

Second Author Dr.UnaiIraola. Computing and Electronics department, University of Mondragon, Arrasate- Mondragon, Spain

Third Author Eng. Jose María Canales. Computing and Electronics department, University of Mondragon, Arrasate-Mondragon, Spain

Forth Author Dr.Ander Goikoetxea. Computing and Electronics department, University of Mondragon, Arrasate- Mondragon, Spain

Fifth Author PhD student. Erik Garayalde Computing and Electronics department, University of Mondragon, Arrasate-Mondragon, Spain